UKAEA FUS 417

EURATOM/UKAEA Fusion

Analysis of vertical displacement events and halo currents in COMPASS-D

P J Knight, C G Castle, A W Morris, A Caloutsis and C G Gimblett

April 1999

EURATOM/UKAEA Fusion Association

Culham Science Centre, Abingdon
Oxfordshire, OX14 3DB
United Kingdom
Telephone +44 1235 464181
Facsimile +44 1235 463647

Analysis of Vertical Displacement Events and Halo Currents in COMPASS–D

P. J. Knight, G. G. Castle[1], A. W. Morris, A. Caloutsis, C. G. Gimblett

Euratom/UKAEA Fusion Association,
Culham Science Centre, Abingdon, Oxon OX14 3DB, United Kingdom

Abstract

Vertical displacement events and their attendant 'halo currents' flowing in the plasma facing components pose a potentially serious hazard to operation in large fusion devices. Experiments on the COMPASS–D tokamak indicate that, on this machine, peak halo currents I_θ exhibit a scaling $I_\theta \propto I_{\rm p0}/q_{95}$, with all data falling within the boundary $I_\theta \leq 1.2 I_{\rm p0}/q_{95}$. Toroidally asymmetric halo currents peak along with the symmetric halo currents, and are nearly fixed in toroidal phase, according to magnetic coil and resistive shunt data. The toroidal peaking factor $\mathcal{P}$ (peak to average ratio) of the halo currents decreases with increasing $I_\theta/I_{\rm p0}$, but exhibits no clear trend. Here, the experimental arrangement is described, and the above results are discussed. A model for the observed boundary in the peak halo current data is introduced, employing near-perfect imaging of the plasma current by a halo that becomes highly conducting during a VDE. The model reproduces both the above limit observed on COMPASS–D and also the higher boundary observed on Alcator C-Mod. In addition, the model results are consistent with reports from other machines of the effectiveness of schemes to reduce halo currents such as gas puffing and killer pellet injection.

1 Introduction

One of the most promising configurations for achieving magnetic fusion is the tokamak of non-circular cross-sectional shape. Such devices possess desirable energy confinement characteristics; however, the same external magnetic fields used to produce the non-circular cross-sectional shape also cause the confined plasma to become unstable to small vertical displacements [1]. In practice, this vertical displacement mode is stabilised by feedback control systems which apply radial magnetic fields to neutralise the plasma motion. In some circumstances the control system may fail, for example due to a large plasma disturbance (such as a large ELM, a change in inductance or pressure due to a reconnection); excessive noise in control signals; increasing instability growth rate exceeding the bandwidth of the controller; or saturation of the power supply in the control loop. The plasma will then move vertically, upwards or downwards depending on the nature of the disturbance/control failure. The plasma current will decay, either as a result of the vertical motion causing contact with the vessel or internal structures and

[1] *Last known address:* University of Texas

subsequent cooling of the plasma core, or as a consequence of the disruptive energy quench that led to the loss of vertical position control. As the plasma current and size decrease, changes in the toroidal and poloidal fluxes induce large (compared to the quiescent values) voltages which in turn drive so-called 'halo currents' in the plasma outside the last closed flux surface and in portions of the vacuum vessel and plasma-facing components (PFCs). This scenario is collectively known as a vertical displacement event, or VDE. The induced currents driven during a VDE are of interest to designers of power plant sized devices since they can produce large mechanical stresses (see Fig. 1) on the conducting components due to interaction with the externally applied magnetic fields. It is important to understand the scaling of these forces and currents to ensure that adequate design measures are incorporated in the construction of future fusion experiments.

2 COMPASS–D experimental arrangement

Halo currents are diagnosed on COMPASS–D by two main diagnostics (see Fig. 2): three toroidally separate arrays of $\dot{B}$ magnetic pickup coils (located at toroidal angles of $\phi = 0$, $\phi = \frac{\pi}{4}$ and $\phi = \pi$ radians) comprising 72 distinct measurements of each field component, and three resistive shunts. The poloidal halo current I_θ flowing along the vacuum vessel wall behind a particular coil is deduced via Ampère's Law as

$$\Delta B_\phi = \frac{\mu_0 I_\theta}{2\pi R} \tag{1}$$

where ΔB_ϕ is the difference between the externally applied toroidal field and the field as measured by integrating the $\dot{B}_\phi$ signal in time from a particular coil. The change in current in the TF coil set is negligible due to their remoteness and large inductance. Fig. 3 shows a typical set of halo current diagnostic traces from a COMPASS–D shot, and clearly demonstrates the energy quench preceding the current quench. Peak poloidal halo currents of up to 0.45 I_{p0} (I_{p0} is the pre–disruption plasma current) have been inferred from magnetic measurements. These values are similar to those seen on ASDEX-U, DIII-D, Alcator C-Mod, JET and JT-60U (Refs. [2]–[21]). The large number of coils provides a unique and powerful diagnostic for halo current measurements. The full set of coils allows determination of both axisymmetric (toroidal mode number $n = 0$) and non-axisymmetric ($n = 1$) current modes with poloidal mode numbers as high as $m = 12$. An example of the poloidal current density distribution, J_θ, in the upper half of the vessel during a VDE (COMPASS–D discharge 17126: $I_{\mathrm{p0}} = 185$ kA, $B_\phi = 1.2$ T) is shown in Fig. 4. One can see several features, including an initial burst of current density in the diamagnetic direction, followed a fraction of a millisecond later by a larger burst of current density in the paramagnetic direction. The poloidal spatial extent of the halo current is also easily observed (in this case covering approximately one radian).

The toroidal current density distribution is determined by two sets of 16 partial Rogowski coils, one set located inside the vacuum vessel, the complementary set located

outside the vacuum vessel (see Fig. 2). The average toroidal current density, $J_\phi(\theta_j)$, in the vessel at a particular poloidal angle θ_j is given by taking the difference in the inner and outer poloidal field values and dividing by the vessel wall thickness d:

$$J_\phi(\theta_j) = \frac{B_\theta^{\text{inner}} - B_\theta^{\text{outer}}}{d}. \tag{2}$$

Fig. 5 displays the toroidal current density distribution during a VDE for COMPASS–D discharge 17126.

3 Observations of halo currents and eddy currents

3.1 Symmetric halo currents

Toroidally symmetric halo currents have been observed to flow during VDEs in several tokamaks [2, 4, 9, 10, 12, 17, 18, 19, 20, 21] and in an RFP [22, 23]. The poloidal halo currents flowing in the vessel interact with the externally applied toroidal field to produce radial and vertical forces on the vacuum vessel. It is important to understand the scaling of these forces and currents to ensure that adequate design measures are incorporated in the construction of future fusion experiments. A variety of plasma shapes were generated on COMPASS–D for VDE experiments: Single Null Diverted (SND), Single Null high Triangularity (SNT), and limiter plasmas (see Fig. 6). Disruptions were also induced both towards and away from the X-point. We determine the toroidally symmetric poloidal halo current distribution by taking the average of the halo current distributions at each of two toroidally opposite sectors. On COMPASS–D, single-parameter scans indicate that the maximum toroidally symmetric poloidal halo currents scale as

$$I_\theta \propto \frac{I_{p0}}{q_{95}} \tag{3}$$

where I_{p0} and q_{95} are the pre-disruption plasma current and the safety factor at 95 % of the last closed flux surface. By 'maximum poloidal halo current' we mean the maximum value of the symmetric poloidal halo current in the paramagnetic direction. The halo current in the diamagnetic direction can be comparable in magnitude to that in the paramagnetic direction, but for COMPASS–D data the paramagnetic halo current is always the largest. Fig. 7 shows the results of several experimental campaigns and illustrates the point that although the individual scalings approximately follow the I_{p0}/q_{95} law, the slopes can differ. Note that five different types of VDE experiment are represented in Fig. 7, involving I_{p0} and B_ϕ scans, induced RMP- (see Section 3.2) and ELM-triggered VDEs, single null diverted (SND, triangularity $\delta \simeq 0.26$) and high triangularity (SNT, $\delta \simeq 0.4$) plasmas. All of the VDEs shown in the plot were downward, towards the X-point, although little difference was found in the data for plasmas moving in either direction [3]. The peak symmetric poloidal halo currents are a strong function of elongation κ, at least up to

$\kappa \sim 1.6$ (see Fig. 8). This result is in agreement with JET data [24], but in contrast to results compiled from several machines [25], which show no direct dependence of halo current on elongation in the range $\kappa \sim 1.5 - 2.0$.

Although individual single-parameter scans exhibit a relatively clean $I_\theta \propto I_{\mathrm{p0}}/q_{95}$ scaling, there is considerable scatter in the halo current data obtained with the same plasma parameters. Fig. 9 depicts the scatter in I_θ when plotted against I_{p0}/q_{95} for a variety of conditions, with varying I_{p0}, B_ϕ and line-averaged density $\overline{n}_{\mathrm{e}}$ as well as both upward and downward disruptions. However, even a subset of the data with fixed B_ϕ and I_{p0} but varying $\overline{n}_{\mathrm{e}}$ displays appreciable scatter. This is not yet fully understood and will be discussed in Section 4.

As the poloidal halo currents may be driven by either poloidal or toroidal electric fields, one expects I_θ to follow $E_\phi \sim \dot{I}_{\mathrm{p}}$, since this is the larger component. Fig. 10 shows that I_θ also follows E_θ ($\sim -I_{\mathrm{p}}\dot{I}_{\mathrm{p}}$).

As the total toroidal and poloidal voltages, V_ϕ and V_θ respectively, are measured directly, secondary inductive effects due to plasma motion, etc., are implicitly included. Also, the smaller diamagnetic halo current preceding the main paramagnetic halo current is consistent with being caused by the energy quench in this case, as only the V_θ trace is in the diamagnetic direction at that time.

Most of the disruptions studied in this paper are 'forced' in the sense that the plasma vertical position control is turned off at a predetermined time and the plasma is given a small push in the desired disruption direction by a small pre-programmed pulse of current in the radial magnetic field coils. VDEs are forced as a means of reliably generating halo current data for various parameter scans. The question arises of whether this technique of forcing intentional VDEs produces results identical to those encountered during unintentional loss of plasma control. To address this issue, we ran two I_{p} scan experiments: one where the VDEs were forced using the method described above, and one where the VDEs were triggered by ELMs. The results of this experiment are shown in Fig. 11. There is no discernible difference in the magnitude of the halo currents, which means the peak halo current values must be insensitive to the cause of the VDE.

The peak halo current is independent of the direction of I_{p0}, and reverses with B_ϕ. This is consistent with observations made on Alcator C-Mod [17] where the halo current reverses direction when both I_{p0} and B_ϕ are reversed (these must be done simultaneously on this machine). This behaviour is expected from both of the important halo current drives, and is discussed below.

3.2 Asymmetric halo currents

Toroidal asymmetries in poloidal halo currents are observed with both magnetic coils and resistive shunts on COMPASS-D. The asymmetric component peaks within tens of μs of the peak of the symmetric halo current, and its toroidal phase is nearly fixed. This is in

contrast to other machines [7, 17] where the asymmetry is seen to rotate at a rate of a few kHz. The asymmetric component is estimated by assuming a toroidal distribution of the form

$$I_\theta(\phi) = I_0 + I_1 \cos(\phi + \psi) \tag{4}$$

where ψ is the toroidal phase of the asymmetry. This expression is fitted to data from three toroidal sectors to obtain the symmetric and asymmetric amplitudes and the phase at the time of peak symmetric halo current I_0. Data fitted in this way are consistent with the values of the halo currents measured by the resistive shunts, which reside at a different toroidal location. The toroidal peaking factor $\hat{\mathcal{P}}$ is the peak halo current divided by the average halo current. In terms of symmetric and asymmetric amplitudes it is given by

$$\hat{\mathcal{P}} = 1 + \frac{I_1}{I_0} \tag{5}$$

$\hat{\mathcal{P}}$ generally decreases for increasing $I_\theta/I_{\rm p0}$, but so far no clear scaling of I_1 has emerged from the data. The general trend of decreasing $\hat{\mathcal{P}}$ with $I_\theta/I_{\rm p0}$ (Fig. 11) suggests either a fixed (or decreasing) growth rate of asymmetry (the larger halo currents being associated with faster $I_{\rm p}$ decays) or a ceiling on the poloidal halo current density J_θ.

The observation that the phase of the halo asymmetry was fixed on COMPASS–D led to the idea that non-uniformities in the vacuum vessel or PFCs were causing a seed instability to grow with a fixed phase. An attempt to alter this initial state was made by applying a Resonant Magnetic Perturbation (RMP) of externally applied magnetic fields with a dominant helicity of $m/n = 2/1$ to produce locked modes. After the modes locked, VDEs were produced by turning off the vertical control. The phase of the locked modes apparently had no effect as a 'seed' perturbation for the halo asymmetry, as neither the phase of the halo current asymmetry nor the magnitude of the symmetric halo current was affected (see Fig. 12). The conditions for these discharges were $I_{\rm p0} = 194$ kA, $B_\phi = 1.2$ T, and $q_{95} = 3.3$.

Detailed modelling of asymmetric halo currents is presented elsewhere (see Ref. [27], and also Refs. [28, 29], in which a mixed-circuit instability is invoked).

4 Analysis of halo current observations

4.1 Diamagnetic and paramagnetic halo current drives

In COMPASS–D a diamagnetic (negative) poloidal halo current is observed to precede the larger paramagnetic (positive) halo current, as seen in Fig. 4. As stated above, this sequence implies that an initial 'thermal quench', when pressure is lost, precedes the final 'current quench', when most of the toroidal plasma current is lost, as seen in other devices.

A thermal quench is often associated with a flattening of the plasma current profile, leading to loss of internal inductance, increase of the plasma current, and a negative

change in toroidal voltage. This translates into diamagnetic halo current, as observed. Furthermore, pressure loss also implies the loss of diamagnetic poloidal plasma current, with back-emfs which also contribute to the diamagnetic halo current.

During the current quench the halo current is paramagnetic and much larger in magnitude, as expected.

Toroidal voltages also drive current in the vessel, independent of the halo current. Comparison of Figs 4 and 5 shows that the toroidal vessel current continues to flow in the negative direction for a short time after the halo current has reversed direction. A simple interpretation is that although the thermal quench is over, and the loss of $I_{\rm p}$ is driving positive current in both halo and vessel, the plasma continues to move towards the vessel, inducing opposing toroidal currents and exceeding the $\dot{I}_{\rm p}$ drive for a while. The halo is probably co-moving with the plasma and is not affected by the motion-related potential.

4.2 Ohm's law for the halo circuit

Magnetic field lines in the halo surface are helical, so that both toroidal and poloidal electric fields drive halo current. To assess the situation we derive a global Ohm's law relating the poloidal halo current I_θ to the toroidal and poloidal voltages V_ϕ, V_θ induced during a VDE (see Appendix A).

The relevant Ohm's law is given by

$$A^{-1}\{\lambda\mathcal{R}_{\rm wall} + (1-\lambda)[1+(qA)^2]\mathcal{R}_{\rm halo}\}\, I_\theta = (1-\lambda)q\, V_\phi + V_\theta\,, \tag{6}$$

where A is the average aspect ratio R/a of the halo and core, q is the edge safety factor, and $\mathcal{R}_{\rm wall}$ and $\mathcal{R}_{\rm halo}$ are the 'unit resistances' (see Appendix A) of the wall and halo regions, respectively. The open magnetic surfaces of the halo do not surround the core completely, leaving open a small fraction λ of the total poloidal perimeter, which is bridged by the conducting wall.

In practice we expect the toroidal drive in Eq. (6) to dominate. To make a simple analytic comparison of the toroidal and poloidal drives, we may write

$$V_\phi = L_\phi \dot{I}_{\rm p} \sim \mu_0 R\,(\ln(8A) - 2)\,\dot{I}_{\rm p}\,, \quad V_\theta = L_\theta \dot{I}_{\rm p\theta} \sim \frac{\mu_0 a^2}{8R}\,\dot{I}_{\rm p\theta}\,, \tag{7}$$

treating the plasma as a conducting ring in the toroidal case, and as a solenoid of radius $\sim a/2$ in the poloidal case. $I_{\rm p\theta}$ is the poloidal plasma current. For a crude estimate of the relative sizes of $I_{\rm p}$ and $I_{\rm p\theta}$ we assume that J_ϕ is constant, so that $B_\theta(r) = (r/a)\,B_\theta(a)$, and that $\mathbf{J}$ is parallel to the field so that $J_\theta/J_\phi = B_\theta/B_\phi$. Taking $B_\phi \sim$ constant, it then follows that

$$\frac{I_{\rm p\theta}}{I_{\rm p}} \sim \frac{1}{q}\,. \tag{8}$$

Relations (7, 8) then give

$$\frac{V_\phi}{V_\theta} \sim 8qA^2\,(\ln(8A) - 2)\,, \tag{9}$$

assuming $\dot{I}_{\rm p}/\dot{I}_{{\rm p}\theta}$ is constant. In COMPASS–D, $A \sim 2.4$, so that the toroidal drive should be larger by much more than an order of magnitude. In the experiment values of $V_\phi > 10$ V and $V_\theta \sim 1$ V are seen (although the latter is partially screened by the vessel). We may therefore neglect the poloidal drive during the current quench.

A further major simplification depends on the relative contributions of the wall and the plasma to the total effective resistance, in the left hand side of Eq. (6). For small λ and large qA, the criterion for neglecting the wall contribution is

$$\frac{(qA)^2}{\lambda}\,\mathcal{R}_{\rm halo} \gg \mathcal{R}_{\rm wall}\,, \tag{10}$$

noting that $(qA)^2/\lambda$ can reach values of ~ 100.

4.3 The halo resistance

If we do neglect the contribution of the wall resistance, and specialise to $qA = B_\phi/B_\theta \gg 1$, the poloidal Ohm's law given in Eq. (6) simplifies to

$$\{qA\mathcal{R}_{\rm halo}\}\, I_\theta = V_\phi\,. \tag{11}$$

Since the halo current flows parallel to the magnetic field,

$$\frac{I_\phi}{I_\theta} = (1-\lambda)q \tag{12}$$

where I_ϕ is the toroidal component of the halo current, and the corresponding toroidal Ohm's law is

$$\{A\mathcal{R}_{\rm halo}/(1-\lambda)\}\, I_\phi = V_\phi\,. \tag{13}$$

The use of Ohm's Law for approximating the halo resistance is quite rigorous, since it avoids the need to estimate the halo temperature as would be required if a Spitzer approach was used.

To validate retrospectively the neglect of the wall resistance, in going from Eq. (6) to Eq. (11), we may use (11) to estimate the halo unit resistance from experimental values of V_ϕ and I_θ. As an example we take shot 17126, which produced a large I_θ. At $t = 0.1519$ s and poloidal angle 0.5 rad, the contour plots of Figs 4 and 5 together with the vessel major radius and thickness from Table 1, indicate that $I_\theta \sim 100$ kA while the toroidal voltage was ~ 50 V. Eq. (11) then yields a halo unit resistance $\mathcal{R}_{\rm halo} \sim 5 \times 10^{-4}/(qA)\ \Omega$. Since $qA > 10$, and the wall unit resistance is, from Table 1, $\mathcal{R}_{\rm wall} \sim 4 \times 10^{-4}\ \Omega$, the halo plasma was, at that time, more conducting than the wall by at least one order of magnitude. Despite this, the criterion for neglecting the wall resistance (Eq. (10)) is still easily satisfied, by two orders of magnitude, due to the large factor $(qA)^2/\lambda$.

It follows that Ohm's law for I_θ is dominated by the halo plasma resistance, despite the fact that the halo plasma itself becomes considerably less resistive than the vessel, especially near peak I_θ.

4.4 Upper limit of the symmetric halo current

One way to determine a maximum value for I_θ is to consider the extreme case where all of the plasma current is lost in a time-scale much shorter than the 'L/R' time-scale of the halo, inducing a flux-preserving halo current.

The previous conclusion, that near the peak I_θ we have $\mathcal{R}_{\rm halo} \ll \mathcal{R}_{\rm wall}$, enables us to neglect the wall contribution in imaging the toroidal plasma current, without loss of accuracy. (The relevant halo toroidal resistance is in fact $\sim A\mathcal{R}_{\rm halo}$, from Eq. (13), but the relevant wall toroidal resistance is likewise $\sim A\mathcal{R}_{\rm wall}$, since only neighbouring parts of the wall will participate effectively.)

Since the halo exactly surrounds the core, the halo and core external toroidal inductances and mutual inductance are the same (the missing perimeter fraction λ is insignificant in calculating inductances), and we may consider a very simple circuit equation

$$I_\phi = -\tau_{\rm halo}(\dot{I}_\phi + \dot{I}_{\rm p}) \tag{14}$$

where $\tau_{\rm halo} = L_{\rm halo}/A\mathcal{R}_{\rm halo}$ is the toroidal 'L/R' time of the halo.

Taking the decay of the driving plasma current as specified, for example as $I_{\rm p} = I_{\rm p0}\exp(-t/\tau_{\rm p})$, it is easy to show that in the limit of a highly conducting halo, when $\tau_{\rm halo} \gg \tau_{\rm p}$, the maximum toroidal halo image current attained is

$$I_\phi^{\rm max} \sim x^{x/(1-x)} I_{\rm p0} \quad \text{where} \quad x \equiv \tau_{\rm p}/\tau_{\rm halo}\,. \tag{15}$$

Note that $x^{x/(1-x)} \to 1$ as $x \to 0$. Losses are insignificant, and $I_\phi^{\rm max} = I_{\rm p0}$ in this limit. Using Eq. (12) to convert to poloidal current we finally find

$$I_\theta^{\rm max} \le (1-\lambda)^{-1} x^{x/(1-x)}\,\frac{I_{\rm p0}}{q}\,, \tag{16}$$

which gives the required upper limit.

According to expression (16), the observed limit corresponds to near-perfect imaging of the plasma current by a halo that becomes highly conducting ($x \ll 1$) during a VDE. The vessel does not participate because it is too resistive, as shown in the previous section. Part of the scatter in the size of I_θ, shown in Fig. 9, may thus be attributed to variation in $\mathcal{R}_{\rm halo}$ itself, and hence in x. This is consistent with the effectiveness of gas puffs, injected to cool the halo plasma, in lowering I_θ — seen in JT-60U experiments [12].

The factor in q is simply geometric, due to the ohmic halo current flowing along the magnetic field. Since $q_{\rm halo} \sim q \sim B_\phi 2\pi a^2/\mu_0 I_{\rm p} R$ (ignoring shaping terms), this dependence strongly suggests that resistive decay of $I_{\rm p}$ occurring while a is still large, at the beginning of a VDE, produces a minimum of halo current per unit plasma current, at all times. This was seen in Alcator C-Mod experiments [26], where a resistive current quench induced early by 'killer-pellets', cooling the plasma, resulted in a marked reduction of the maximum halo current.

The factor in $(1-\lambda)$ is due to the missing poloidal perimeter of the halo plasma, which means that the toroidal halo image current is squeezed inside the remaining perimeter, raising the toroidal current density.

Expression (16) seems in line with experimental data. In both COMPASS–D and Alcator C-Mod [2, 3, 17] the maximum I_θ is bounded by $I_\theta^{\max} \sim C_0 I_{\rm p0}/q_{95}$. For COMPASS–D, $C_0 \sim 1.2$, while for Alcator C-Mod, $C_0 \sim 1.6$ [17]. Looking at the flux contours of Fig. 6 we may suppose that in COMPASS–D λ is rather small, $\sim 1/8$ very roughly, which would give a $C_0 = (1-\lambda)^{-1} \sim 1.2$. For Alcator C-Mod, Figure 3 of [17] clearly indicates that a larger λ, perhaps $\sim 3/8$ is reached, because of the different configuration, so that $C_0 \sim 1.6$, or more, is anticipated.

5 Summary

It has been observed on COMPASS–D that single parameter scans ($I_{\rm p0}$, B_ϕ, κ) of peak halo current I_θ exhibit a scaling $I_\theta \propto I_{\rm p0}/q_{95}$, with all data falling within the boundary $I_\theta \leq 1.2 I_{\rm p0}/q_{95}$. A model for this boundary has been developed, employing near-perfect imaging of the plasma current by a halo that becomes highly conducting during a VDE. The model reproduces both the above limit observed on COMPASS–D and also the higher boundary observed on Alcator C-Mod. In addition, the model results are consistent with the reported effectiveness of schemes to reduce halo currents such as gas puffs in JT-60U and killer pellets in Alcator C-Mod.

Toroidally asymmetric halo currents on COMPASS–D are nearly fixed in toroidal phase, according to both magnetic coil and resistive shunt data. It should be noted that the maximum toroidal peaking factor $\hat{\mathcal{P}}$ (peak to average ratio) and peak $I_\theta/I_{\rm p0}$ do not coincide in time in general. There is no clear scaling of $\hat{\mathcal{P}}$ (measured at the time of maximum $I_\theta/I_{\rm p0}$) with $I_\theta/I_{\rm p0}$, although some tendency to fall with $I_\theta/I_{\rm p0}$ (increase with increasing q) is observed. This behaviour would be favourable for tokamak design as it indicates local stresses will not increase in proportion to the symmetric halo current. More detailed modelling of asymmetric halo currents is presented elsewhere ([27]–[29]).

Acknowledgements

The authors would like to thank the COMPASS–D team for their work on the instrumentation and maintenance of the halo current diagnostics. This work was funded by the UK Department of Trade and Industry and Euratom.

Appendix A: Application of Ohm's Law to the Halo in a Circular Cross-section Plasma

We consider a model of a simple halo, where the plasma core and halo have an average aspect ratio $A = R/a$, with a the minor plasma radius, and an edge $q \sim q_{\rm halo}$. The open magnetic surfaces of the halo do not surround the core completely, leaving open a small fraction λ of the total poloidal perimeter, which is bridged by the conducting wall. The halo and the wall have 'unit resistances' defined as $\mathcal{R}_{\rm halo/wall} \equiv (\sigma_{\rm halo/wall} w_{\rm halo/wall})^{-1}$ where w denotes the width of the given region.

The local Ohm's law in the halo, applied parallel to the field, gives

$$J_{||} = \sigma_{\rm halo}[E_\phi \sin a + E_\theta \cos a] \tag{A1}$$

where $\tan a = B_\phi / B_\theta = qA$. We relate the electric fields to potential drops by adopting average values of the major and minor halo radii, so that

$$E_\phi \sim \frac{V_\phi}{2\pi R} \quad \text{and} \quad E_\theta \sim \frac{V_\theta^{\rm PQ}}{2\pi a(1-\lambda)} \,. \tag{A2}$$

Points P, Q are the poloidal locations of the inboard and outboard plasma-wall contacts, so that PQ is the poloidal arc defined by the halo, whereas QP is the short way along the vessel, completing the poloidal circuit. Also introducing the halo current by

$$I_\theta = 2\pi R\, w_{\rm halo} J_\theta \quad \text{and} \quad J_\theta = J_{||} \cos a \,, \tag{A3}$$

relation (A1) may be put in the form

$$\frac{1-\lambda}{A\cos^2 a}\, \mathcal{R}_{\rm halo} I_\theta = \frac{(1-\lambda)\tan a}{A}\, V_\phi + V_\theta^{\rm PQ} \,. \tag{A4}$$

Turning to the wall sector, Ohm's law in the poloidal direction gives

$$V_\theta^{\rm QP} = \frac{2\pi a \lambda}{\sigma_{\rm wall} w_{\rm wall} 2\pi R}\, I_\theta = \frac{\lambda \mathcal{R}_{\rm wall}}{A}\, I_\theta \,. \tag{A5}$$

Current continuity is observed by the use of the same poloidal current, I_θ, for both wall and halo poloidal circuits. It is thus assumed that poloidal current flowing the long way around the vessel is negligible. Finally, around the core, we have

$$V_\theta = V_\theta^{\rm PQ} + V_\theta^{\rm QP} \tag{A6}$$

so that elimination of $V_\theta^{\rm PQ}, V_\theta^{\rm QP}$ between relations (A4 – A6) gives the required Ohm's law

$$A^{-1}\{\lambda \mathcal{R}_{\rm wall} + (1-\lambda)[1+(qA)^2]\mathcal{R}_{\rm halo}\}\, I_\theta = (1-\lambda) q\, V_\phi + V_\theta \,. \tag{A7}$$

This neglects evolution of the toroidal vacuum field, which is small in COMPASS–D due to the large size of the TF coils with respect to the plasma.

References

[1] LAZARUS, E.A., LISTER, J.B., NEILSON, G.H., Nucl. Fusion **30** (1990) 111.

[2] CASTLE, G.G., et al., in Controlled Fusion and Plasma Physics (Proc. 23rd Eur. Conf. Kiev, 1996), Vol. **20C**, Part I, European Physical Society, Geneva (1996) 420.

[3] CASTLE, G.G., et al., in Fusion Energy (Proc. 16th Int. Conf. Montreal, 1996), Vol. **1**, IAEA, Vienna (1997) 707.

[4] GRUBER, O., LACKNER, K., PAUTASSO, G., SEIDEL, U., STREIBL, B., Plasma Phys. Control. Fusion **35** (1993) 191.

[5] GRUBER, O. *"Asymmetries during Disruptions and Interaction with the Structures in ASDEX Upgrade"*, paper presented at Tripartite Exchange Agreement Workshop on Effects of Plasma Behaviour on Tokamak Structural Components, JET, Abingdon, 1996.

[6] TAYLOR, P.L., et al., *"DIII-D Disruption Studies"*, paper presented at Disruption and Vertical Displacement Event Characterization Workshop, ITER Joint Work Site, Garching, 1995.

[7] SCHAFFER, M.J., et al., *"VDE Halo Current, Asymmetric Forces, and Mitigation in DIII-D"*, paper presented at Tripartite Exchange Agreement Workshop on Effects of Plasma Behaviour on Tokamak Structural Components, JET, Abingdon, 1996.

[8] EVANS, T. E., et al., in J. Nucl. Materials (Proc. 12th Int. Conf. on Plasma-Surface Interactions in Controlled Fusion Devices, St-Raphael, 1996), Vols. **241–243** (1997) 606.

[9] HYATT, A.W., et al., in Controlled Fusion and Plasma Physics (Proc. 23rd Eur. Conf. Kiev, 1996), Vol. **20C**, Part I, European Physical Society, Geneva (1996) 287.

[10] ANDREW, P., et al., in Fusion Engineering (Proc. 16th Symp. Champaign, 1995), IEEE, Piscataway, NJ (1995).

[11] NOLL, P., *"Tentative Interpretation of Plasma Behaviour Leading to Forces on Structural Components"*, paper presented at Tripartite Exchange Agreement Workshop on Effects of Plasma Behaviour on Tokamak Structural Components, JET, Abingdon, 1996.

[12] YOSHINO, R., et al., Nucl. Fusion **33** (1993) 1599.

[13] YOSHINO, R., et al., in Fusion Energy (Proc. 15th Int. Conf. Seville, 1994), Vol. **1**, IAEA, Vienna (1995) 685.

[14] NEYATANI, Y., YOSHINO, R., ANDO, T., Fusion Technol. **28** (1995) 1634.

[15] NAITO, O., YOSHINO, R., NEYATANI, Y., NAKAMURA, Y., Proceedings of the Workshop on Effects of Plasma Behaviour on Tokamak Structural Components, 10–12 Sept. 1996.

[16] PAUTASSO, G., HERRMANN, A., et al., Nucl. Fusion **34** (1994) 455.

[17] GRANETZ, R.S., et al., Nucl. Fusion **36** (1996) 545.

[18] CHOE, W., et al., in Controlled Fusion and Plasma Physics (Proc. 24th Eur. Conf. Berchtesgaden, 1997), Vol. **21A**, Part III, European Physical Society, Geneva (1997) 1197.

[19] JANOS, A., et al., Proc. ITER EDA Disruption Expert Group Workshop, Garching, Germany, February 13–17, 1995.

[20] SAUTHOFF, N.R., et al., *"PBX-M Disruption and Vertical Displacement Event Characterization"*, paper presented at Disruption and Vertical Displacement Event Characterization Workshop, ITER Joint Work Site, Garching, 1995.

[21] NEYATANI, Y., et al., to be published in Fusion Energy (Proc. 17th Int. Conf. Yokohama, 1998), IAEA, Vienna (1999).

[22] PERUZZO, S., BARTIROMO, R., POMARO, N., SONATO, P., in Controlled Fusion and Plasma Physics (Proc. 24th Eur. Conf. Berchtesgaden, 1997), Vol. **21A**, Part I, European Physical Society, Geneva (1997) 341.

[23] PERUZZO, S., et al., in Fusion Technology (Proc. 19th Symp. Fusion Technology, Lisbon, 1996), Vol. **1**, North-Holland, Amsterdam (1997) 767.

[24] WESLEY, J., et al., in Fusion Energy (Proc. 16th Int. Conf. Montreal, 1996), Vol. **2**, IAEA, Vienna (1997) 971.

[25] YOSHINO, R., et al., to be published in Fusion Energy (Proc. 17th Int. Conf. Yokohama, 1998), IAEA, Vienna (1999).

[26] GRANETZ, R.S., et al., in Fusion Energy (Proc. 16th Int. Conf. Montreal, 1996), Vol. **1**, IAEA, Vienna (1997) 757.

[27] POMPHREY, N., BIALEK, J. M., PARK, W., Nucl. Fusion **38** (1998) 449.

[28] CALOUTSIS, A., GIMBLETT, C.G., Nucl. Fusion **38** (1998) 1487.

[29] CALOUTSIS, A., GIMBLETT, C.G., in Controlled Fusion and Plasma Physics (Proc. 25th Eur. Conf. Prague, 1998), Vol. **22C**, European Physical Society, Geneva (1998) 1963.

name	value	units
conductivity σ	7.94×10^5	$\Omega^{-1}\,\mathrm{m}^{-1}$
wall thickness d	0.003	m
major radius R_0	0.557	m
horizontal minor radius a	0.232	m
vertical minor radius b	0.384	m
toroidal resistance R_ϕ	696	$\mu\Omega$
poloidal resistance R_θ	227	$\mu\Omega$
toroidal inductance L_ϕ	0.97	μH
L/R time of first vertically asymmetric eigenmode	0.37	msec
L/R time of first horizontally asymmetric eigenmode	0.73	msec

Table 1: *Summary of COMPASS-D vessel parameters. The L/R times refer to the eigenvalues of the toroidal current density modes of the vacuum vessel. The first vertically asymmetric mode is primarily excited in response to vertical motions of the plasma or to changes in I_p for plasmas vertically displaced from the vessel centre.*

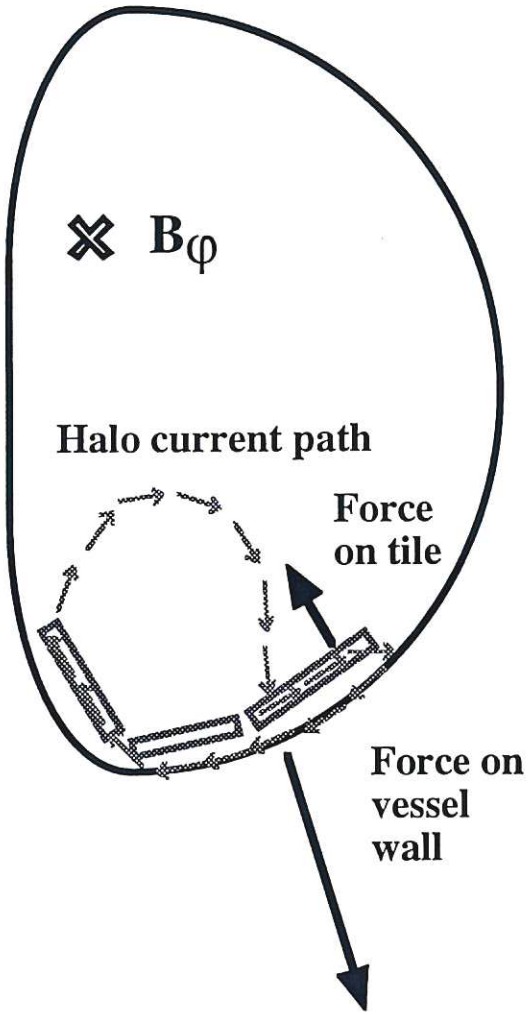

Figure 1: *Figure indicating possible path of poloidal halo currents. The poloidally flowing halo currents interact with the externally applied toroidal magnetic field to produce forces on both the vacuum vessel wall and any plasma-facing components which comprise part of the halo current circuit. Toroidal non-uniformities in the vessel conductivity (like ports, antennae, etc.) will cause local variations in the halo current pattern and hence produce local stresses.*

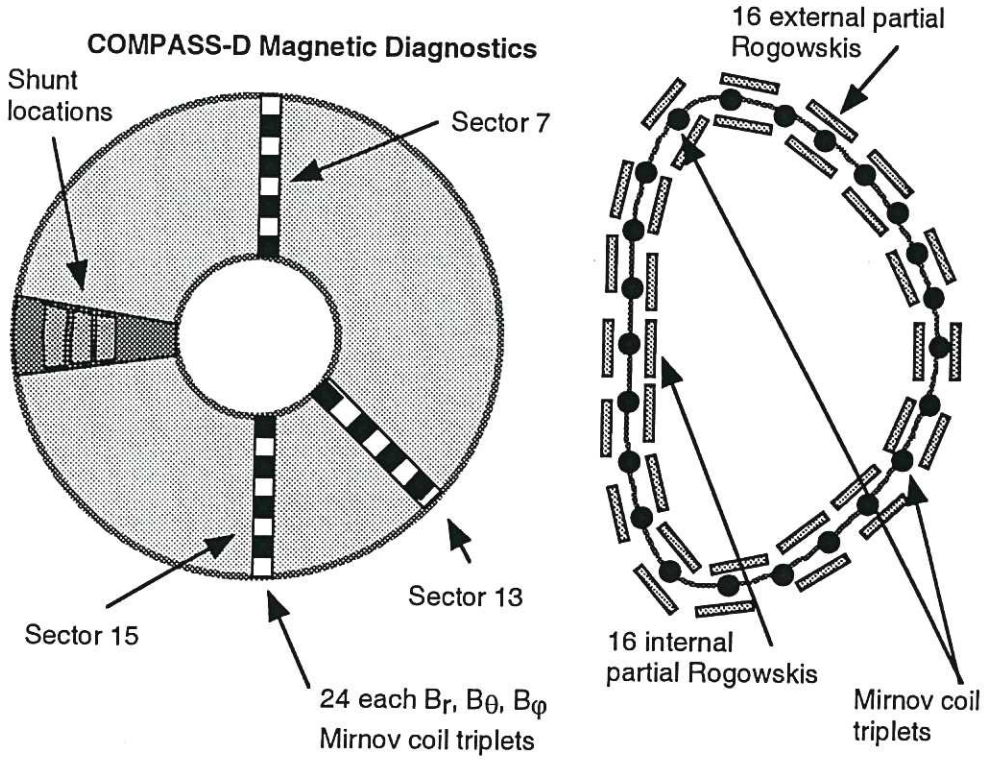

Figure 2: *Diagram indicating COMPASS–D magnetic diagnostic coil locations. Sector 15 corresponds to* $\phi = 0$ *(*ϕ *increases in the counter-clockwise direction), with sectors 13 and 7 at toroidal angles of* $\phi = \frac{\pi}{4}$ *and* $\phi = \pi$*, respectively. The poloidal angle* θ *is equal to zero on the outside midplane and increases in the counter-clockwise direction.*

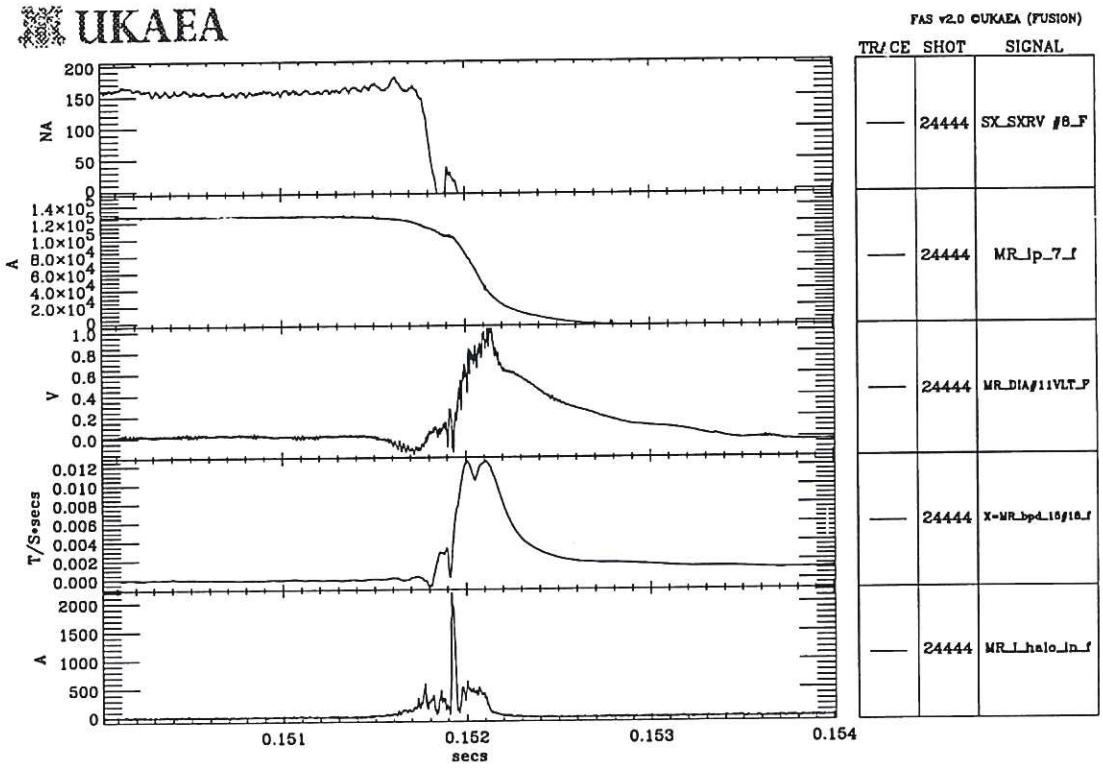

Figure 3: *Summary of diagnostics traces during shot 24444. The traces are as follows, from top to bottom: vertically viewing central SXR brightness (a measure of the plasma energy), plasma current, poloidal voltage as measured by a diamagnetic loop, ΔB_ϕ from a magnetic pickup coil (proportional to poloidal halo current) and the current through a resistive shunt connecting a tile and the vacuum vessel.*

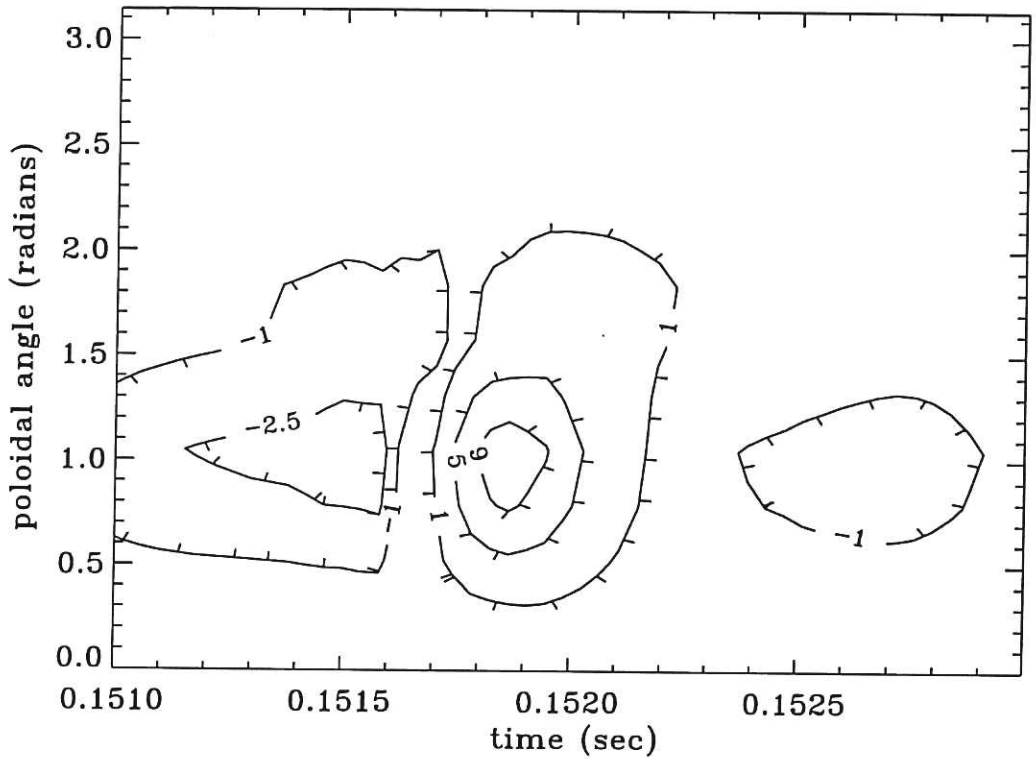

Figure 4: *Contour plot of poloidal halo current density J_θ as a function of time and poloidal angle for the top half of the COMPASS–D vessel for discharge 17126 (an upward VDE). The values marked are in units of MA/m^2 (tick marks indicate the direction of decreasing values). One can clearly see the halo current flowing in the diamagnetic sense (negative contour values) then changing direction and peaking with a substantially larger magnitude approaching* ~ 100 *kA.*

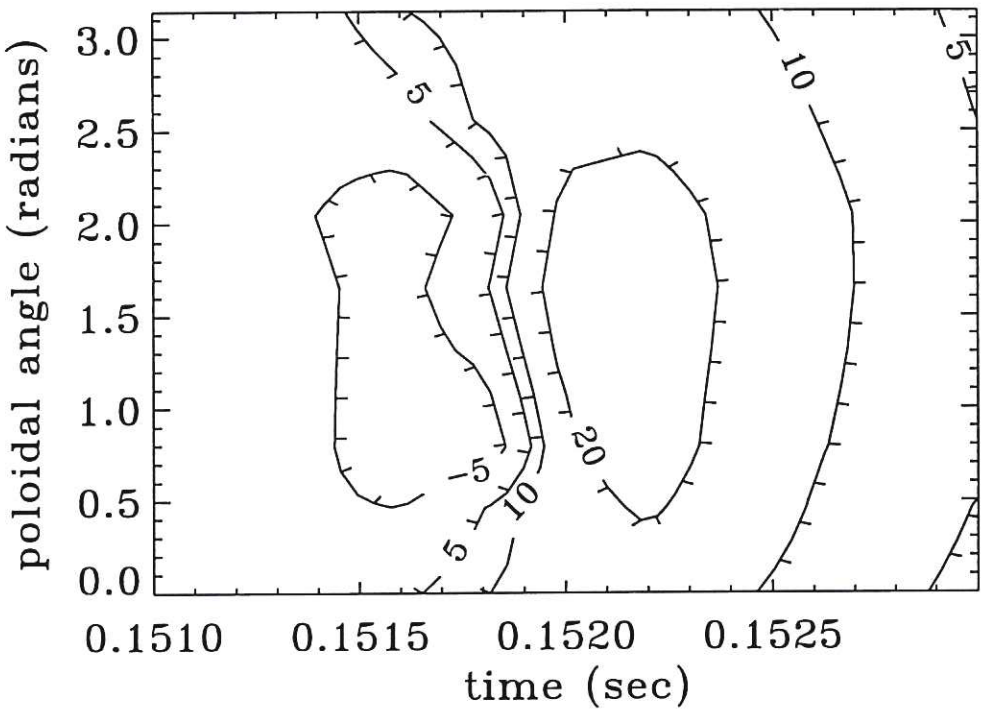

Figure 5: *Contour plot of toroidal halo current density J_ϕ as a function of time and poloidal angle for the top half of the COMPASS–D vessel for discharge 17126 (an upward VDE). The values marked are in units of MA/m^2. At the time of peak poloidal halo current density (see Fig. 4) the toroidal voltage driving $J_\phi \sim 10$ MA/m^2 is ~ 50 V, given the wall conductivity and vessel major radius values listed in Table 1.*

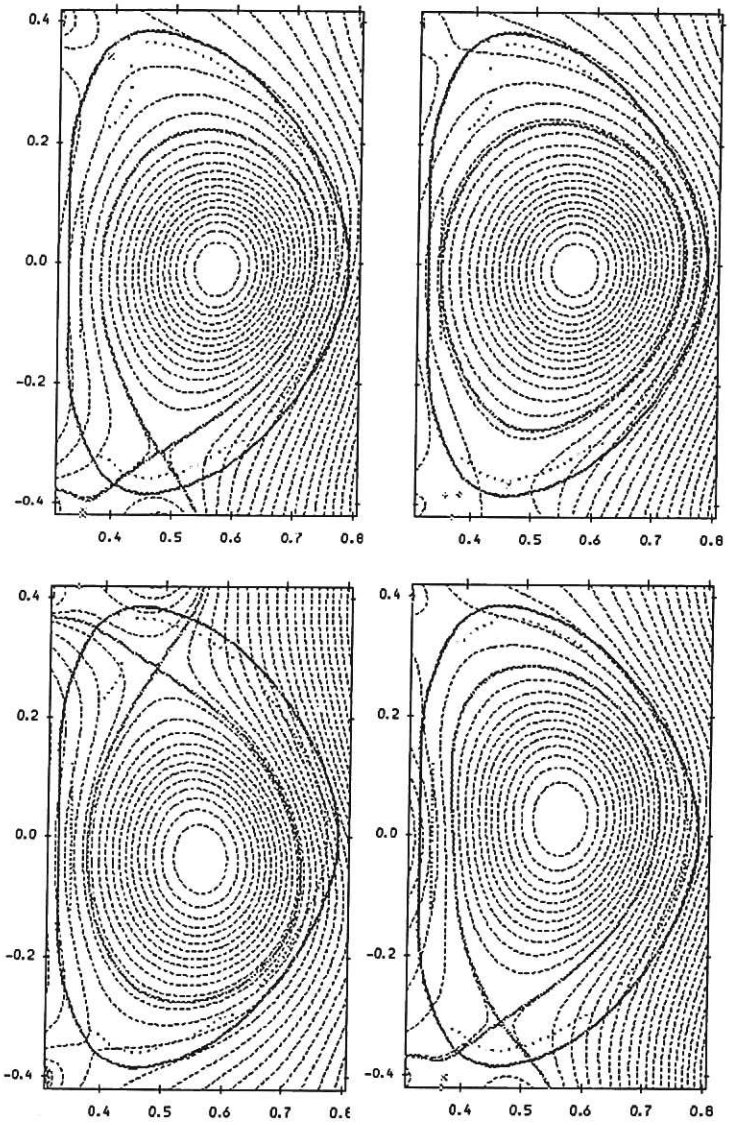

Figure 6: *A variety of plasma equilibria are employed in the study of VDEs and halo currents on COMPASS-D. Shown above are Single Null Diverted plasmas with top and bottom X-points, high triangularity ($\delta \simeq 0.4$) and undiverted equilibria. In addition, high β_p, $\overline{n}_e$ limit, ELM-induced (both L- and H-mode) and control failure VDEs were studied. Parameters ranged from $q_{95} = 2.4 - 8.9$, $I_{p0} = 95 - 239$ kA, and $B_\phi = 0.73 - 1.86$ T.*

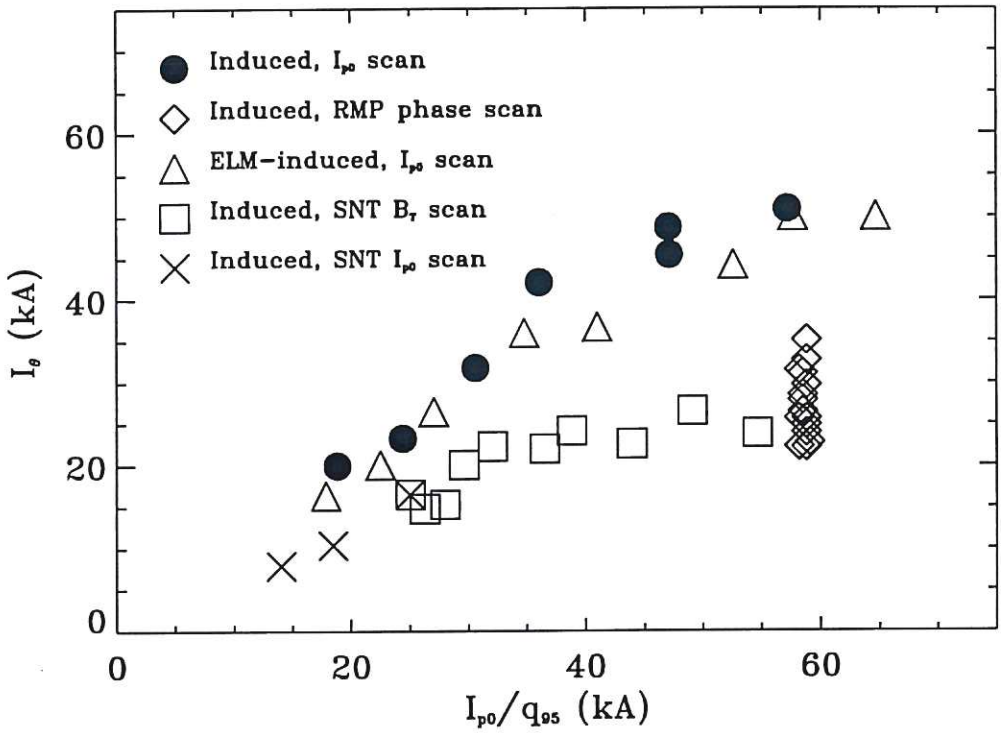

Figure 7: *The scaling of poloidal halo current I_θ as a function of I_{p0}/q_{95} for several different experimental runs. In all cases, the VDEs were either induced by turning off the vertical position feedback control, or by ELMs. Induced, I_{p0} scan conditions: $I_{p0} = 107 - 189$ kA, $B_\phi = 1.2$ T, $q_{95} = 3.3 - 5.7$. Induced, RMP phase scan conditions: $I_{p0} = 194$ kA, $B_\phi = 1.2$ T, $q_{95} = 3.3$. ELM-induced, I_{p0} scan conditions: $I_{p0} = 109 - 207$ kA, $B_\phi = 1.3$ T, $q_{95} = 3.2 - 6.1$. Induced, SNT B_ϕ scan conditions: $I_{p0} = 170$ kA, $B_\phi = 0.7 - 1.7$ T, $q_{95} = 3.0 - 6.9$. Induced, SNT I_{p0} scan conditions: $I_{p0} = 125 - 173$ kA, $B_\phi = 1.7$ T, $q_{95} = 6.9 - 8.9$.*

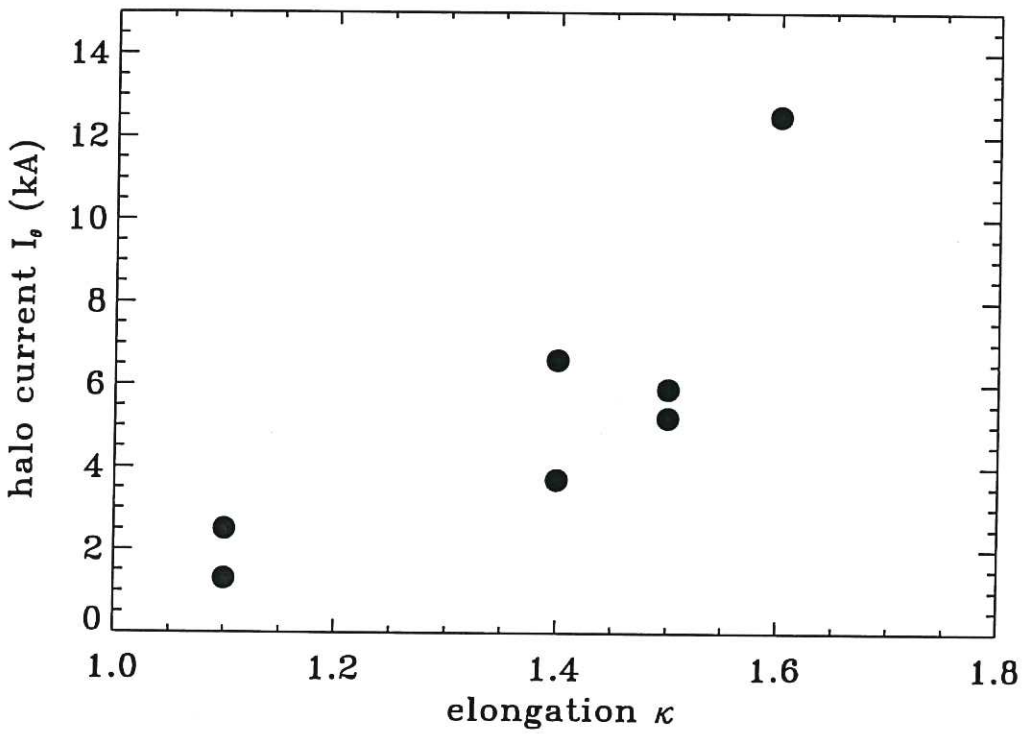

Figure 8: *Scaling of peak poloidal halo current I_θ with elongation κ, showing a strong dependence. The conditions for this scan were $I_{p0} = 137$ kA, $B_\phi = 1.2$ T.*

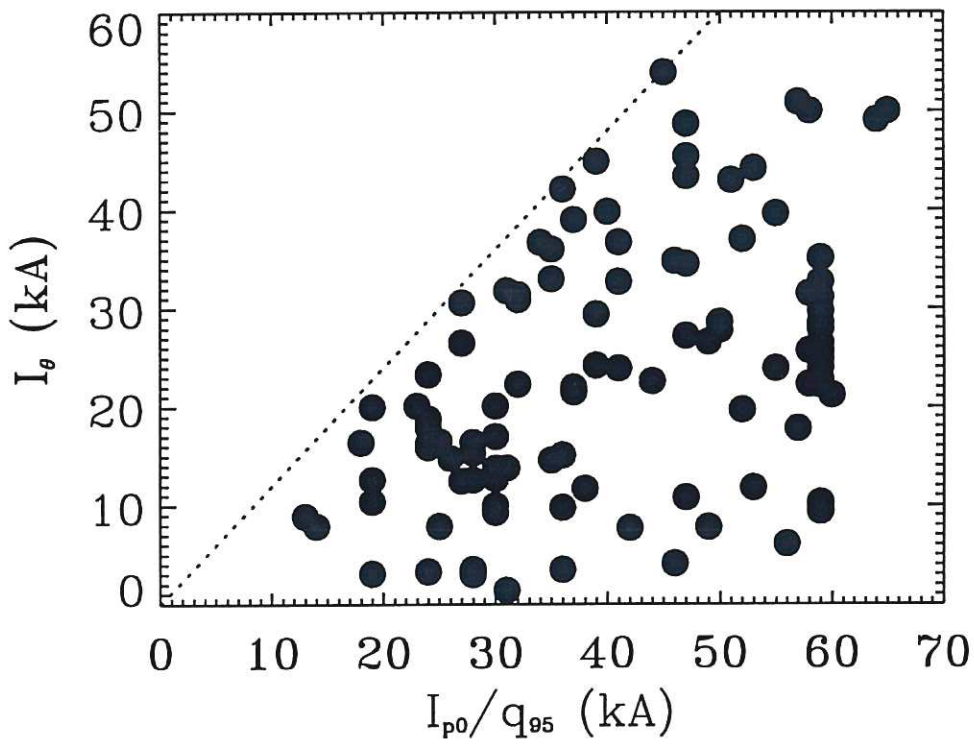

Figure 9: *The maximum poloidal halo current I_θ as a function of I_{p0}/q_{95} for a variety of conditions. The dashed line indicates the upper limit of $I_\theta^{max} \sim 1.2 I_{p0}/q_{95}$.*

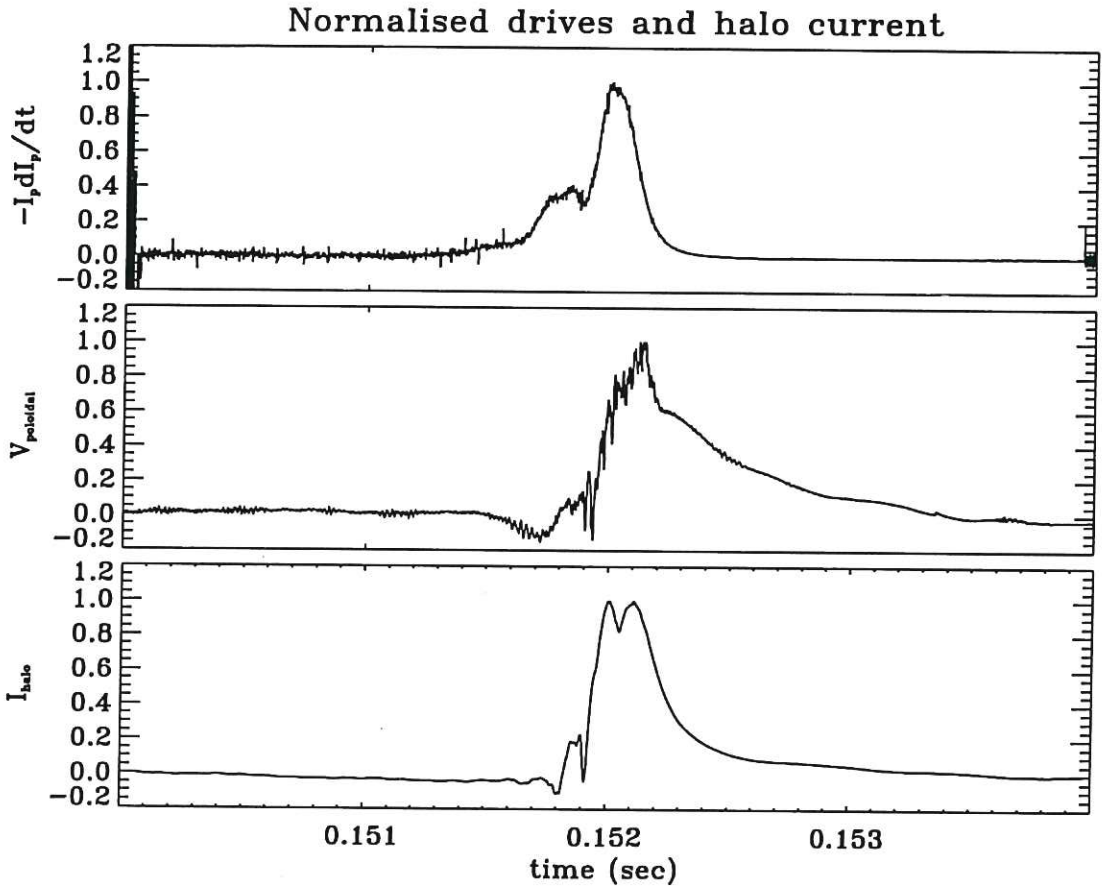

Figure 10: *Figure indicating the primary poloidal halo current drives for COMPASS–D discharge 24444. The top trace is $-I_p\dot{I}_p$, the middle is the poloidal loop voltage V_θ measured by a diamagnetic loop, and the bottom trace is the poloidal halo current I_θ from ΔB_ϕ measured by a magnetic pickup coil (all here divided by their maximum values). The conditions for this discharge were $I_{p0} = 140\ kA$, $B_\phi = 1.15\ T$, $\overline{n}_e = 2.5 \times 10^{19}\ m^{-3}$, $q_{95} = 4.4$.*

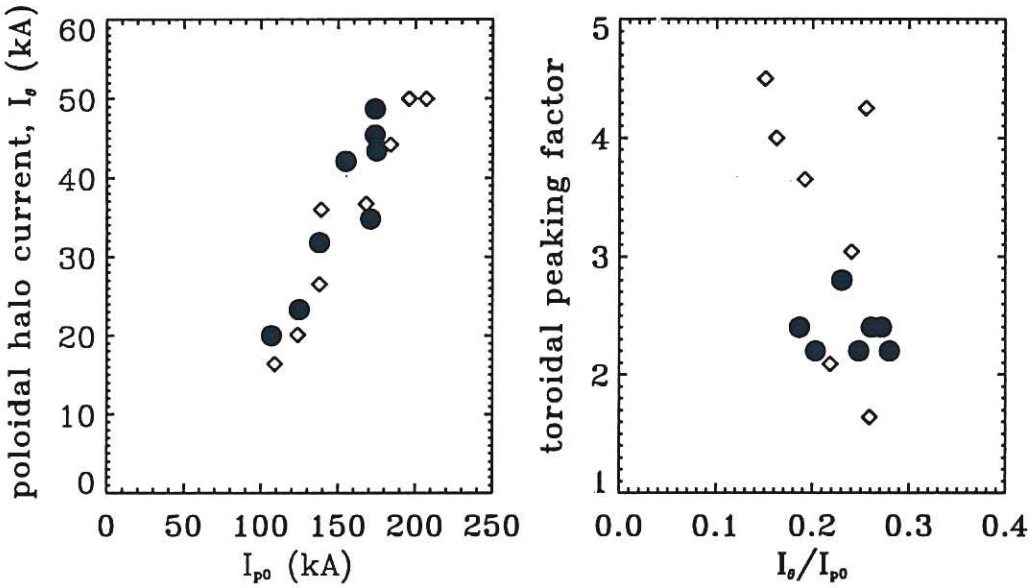

Figure 11: *Comparison of ELM-induced (open diamonds) and forced disruptions (solid circles) for a series of discharges with $B_\phi = 1.2$ T ($\kappa = 1.6$). The magnitudes of the toroidally symmetric poloidal halo currents are virtually identical in each case, but there is significant scatter in the toroidal peaking factor values for the ELM-induced VDEs.*

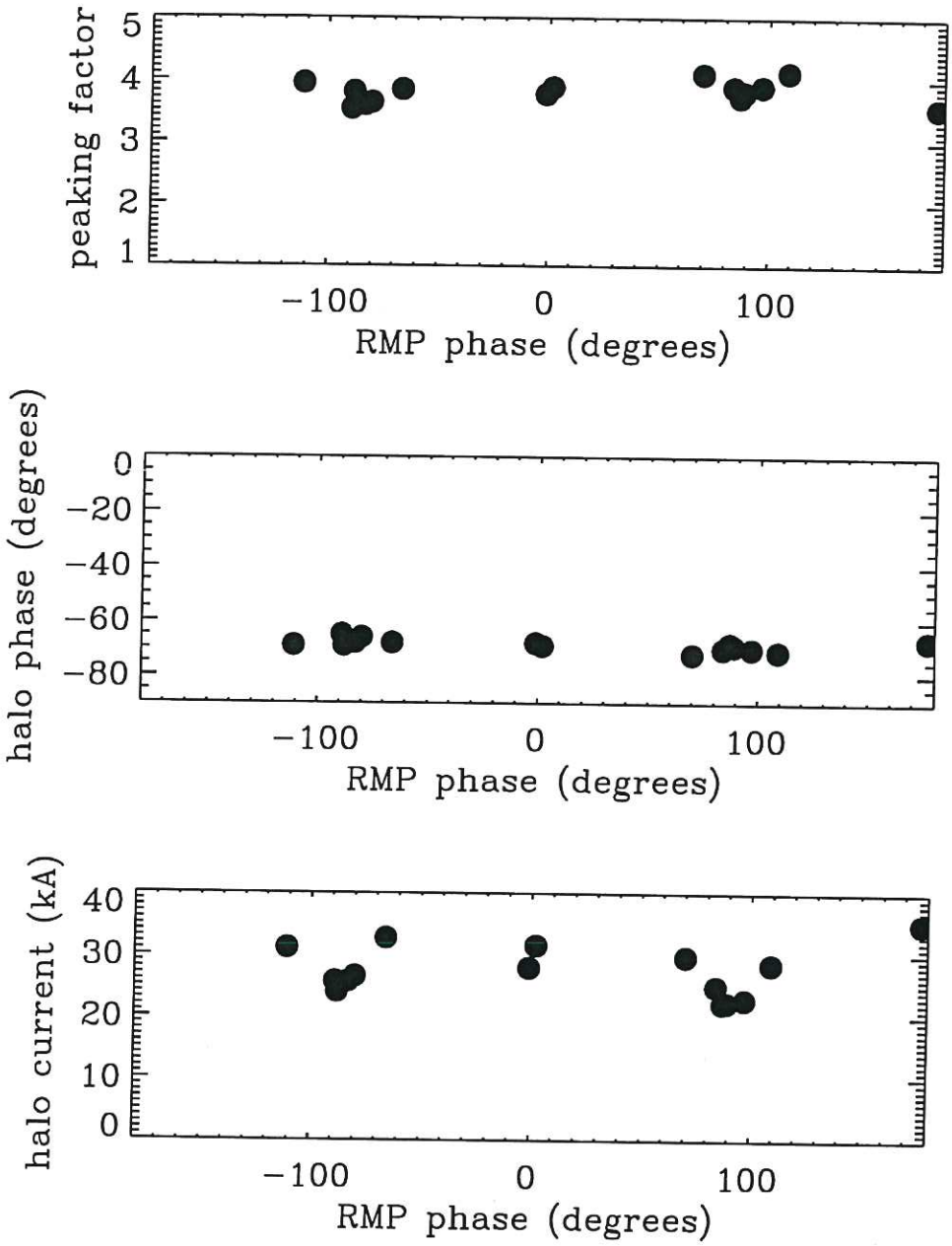

Figure 12: *Data from a Resonant Magnetic Perturbation (RMP) experiment where externally applied magnetic fields with a dominant helicity of $m/n = 2/1$ were applied to produce locked modes. After the modes locked, VDEs were produced by turning off the vertical control. The phase of the locked modes apparently had no effect as a 'seed' perturbation for the halo asymmetry, as neither the phase of the halo current asymmetry nor the magnitude of the symmetric halo current was affected. The conditions for these discharges were $I_{p0} = 194\ kA$, $B_\phi = 1.2\ T$, and $q_{95} = 3.3$.*